ISSN 1070-3632, Russian Journal of General Chemistry, 2013, Vol. 83, No. 12, pp. 2465–2471. © Pleiades Publishing, Ltd., 2013.

Soft Chemistry Synthesis and Properties of Silver Orthophosphate Powders[1]

I. Bozetine[a], Y. Boukennous[a], N. Moudir[a], B. Bellal[b], and M. Trari[b]

[a] *Semiconductors Technology Research Centre for Energetics, 2 Boulevard Frantz Fanon, BP 140 Alger-7 Merveilles, Algiers, Algeria*

[b] *Laboratory of Storage and Renewable Energies (USTHB), Faculty of Chemical 32, Algiers, 16111 Algeria*
e-mail: solarchemistry@gmail.com

Received May 16, 2013

Abstract— Silver orthophosphate powders with superior quality used in phosphorus-doped conductive pastes for solar cell metallization were obtained by precipitation from phosphate precursors. The powders were investigated by X-ray diffraction, scanning electron microscopy coupled with energy dispersive spectrometry, Fourier-transform infrared spectroscopy, thermal analysis, and diffuse reflectance spectroscopy. Spherical silver orthophosphate particles with a size of 0.8 to 10 μm were obtained by chemical precipitation, and the compound crystallized in a cubic symmetry. Relatively smaller crystallites were obtained from disodium hydrogen phosphate. The optical gap determined from the diffuse reflectance spectra using the Kubelka-Munk function varied between 2.05 and 2.30 eV. The electrical conductivity is characteristic of a semiconducting behaviour with activation energy of 0.20 eV. To improve the metal–semiconductor interface, the uniformity of powders of the deposited paste must be enhanced.

DOI: 10.1134/S107036321312044X

INTRODUCTION

Photovoltaic solar devices based on polycrystalline materials exhibit inhomogeneous structural and electrical properties. Characteristics of these devices depend on the fabrication process. In particular, the nature of the metallization paste and the quality of the resulting front electrical contacts will considerably affect the overall energy conversion efficiency. Electric contacts are obtained using the screen-printing technology [1, 2] which reduces the fabrication time, the number of process steps, and the energy consumption when compared to other deposition methods. Therefore, this technique offers the advantage of low cost for solar cell fabrication [3, 4]. Metallization paste is the major efficiency-limiting and cost-determining step in solar cell production [5]. Production of high quality solar cells requires a good knowledge of physicochemical properties of the paste. Therefore, the optical and electrical properties of solar cells should be optimized as a function of the paste properties. Silver orthophosphate (Ag_3PO_4) powder is added to the silver paste used in the metallization of the front contact to improve electrical conductivity.

Selective emitter has been used to reduce the contact resistance due to heavy doping underneath the metal grid [6]. Furthermore, the front-surface passivation of the lightly doped region below the grid is improved and the recombination rate under the metal contact is reduced [6]. However, a good quality of selective emitter is difficult to achieve via one process step. Recently, new innovative approaches to form a selective emitter cell using screen-printing have been reported [7–10]. Three screen-printing approaches have been used in the past: (*i*) selective-emitter cells fabricated via masking and etching [7], (*ii*) selective-emitter cells fabricated by self-alignment with no masking or etching [8], and (*iii*) selective-emitter cells fabricated by self-aligned and self-doping Ag pastes [9, 10]. The main electric power losses are due to the grid shadow and particularly that related to the series resistance (R_s). In order to minimize the resistance R_s, the grid dimensions, as well as the nature and the firing process of the pastes, must be optimized. The grid must occupy a small surface in order to collect most incident photons for a maximum power output.

Screen-printing techniques (*i*) and (*ii*) provide good performance but are time-consuming and relatively more expensive [11]. By contrast, technique (*iii*) is

[1] The text was submitted by the authors in English.

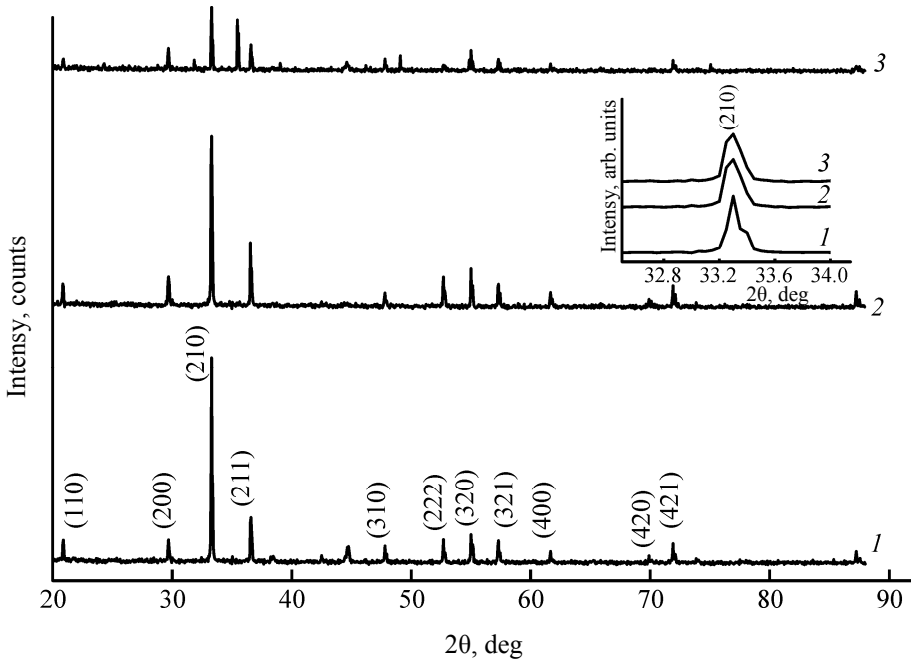

Fig. 1. XRD spectra of Ag_3PO_4 powder samples obtained from different precursors: (a) PA1, (b) PA2, and (c) PA3.

relatively easier to implement on large-scale prodution. If the electric contact obtained by this technique is improved, it could lead to reduction of the solar cell cost per unit power. We have prepared a phosphorus-containing conductive paste with optimized composition for grid metallization. Submicron Ag_3PO_4 particles readily precipitate as bright yellow crystalline material which exhibits a relatively high thermal stability. Submicron particles provide numerous optoelectronic advantages [12]. More interestingly, these powders provide a uniform paste composition and tunable electric and optical properties.

Synthesis of high quality Ag_3PO_4 powder is not straightforward. Chemical precipitation has been used in the past as it allows a better control of the morphology. Indeed, it provides a narrow size distribution and small crystallite size. However, it has not yet been established whether the precursor composition directly affects the crystallite size and morphology of the synthesized particles. The resulting powders are nominally stoichiometric when prepared at an Ag/P molar ratio of 1 : 1, and this approach has been shown to prevent agglomeration and segregation [13]. The aim of this work was to prepare Ag_3PO_4 particles from different precursors to obtain insights on how they influence the physical, optical, and electrical properties.

EXPERIMENTAL

A slightly modified chemical process described elsewhere [14] was used to prepare silver orthophosphate Ag_3PO_4. Crystalline powder consisting of ultrafine particles was obtained by precipitation from $AgNO_3$ and disodium hydrogen phosphate Na_2HPO_4, potassium dihydrogen phosphate KH_2PO_4, or phosphoric acid H_3PO_4, all reactants being of analytical grade. Solutions were prepared using doubly distilled water. Fresh solutions containing the desired proportions of $AgNO_3$ (1 M) were prepared, and phosphate precursor (1 M) was added dropwise at room temperature under moderate magnetic agitation (1200 rpm). The yellow precipitate was separated by centrifugation (5000 rpm, 10 min), thoroughly washed with water, and dried at 80°C. The powders obtained by mixing with Na_2HPO_4, KH_2PO_4 and H_3PO_4 were labeled as PA1, PA2, and PA3, respectively.

Crystalline phases were identified by X-ray diffraction (Bruker D8 Advance diffractometer; CuK_α radiation, λ = 0.154178 nm; scan rate 2θ/min in 0.05° steps with a 10-s counting time for each step). A set of complementary techniques was used to characterize the powders. The thermal analysis was performed on a Setaram thermogravimetric analyzer (TGA) at a heating rate of 2 deg/min. The differential scanning

Some characteristics of silver orthophosphate powders obtained from different precursors

Sample (precursor)	Lattice constant, Å	Cristallite size, nm	Grain size, μm	Optical gap, eV	$\bar{\nu}$, cm^{-1}
PA1 (Na_2HPO_4)	6.0038	77	0.8–0.9	2.30	1005.02
PA2 (KH_2PO_4)	6.0149	63	1.5	2.06	1004.48
PA3 (H_3PO_4)	6.0120	62	10	2.05	1005.78

calorimetry (DSC) was done with a Netzsch DSC 404 C thermal analyzer at a heating rate of 5 deg/min over the range from 20 to 800°C. The IR spectra were recorded in KBr with a Thermo-Nicolet 380 Fourier-transform infrared (FTIR) spectrometer in the range from 400 to 4000 cm^{-1}. The powder morphology was examined by scanning electron microscopy (SEM) using a Phillips XL30 microscope. The compositional analysis was carried out by energy dispersive spectroscopy (EDS) at an accelerating voltage of 25 kV. The diffuse reflectance spectra were recorded with a Varian Cary 500 spectrophotometer. The electrical resistivity was measured by the four-probe technique on a sintered pellet (500°C, 3 h) using an Agilent 4263B LCR Meter; the current within the electrical circuit was kept constant at 1 mA.

RESULTS AND DISCUSSION

The chemical homogeneity and stoichiometry of Ag_3PO_4 powders depend on the details of their synthesis and post-synthesis processes. We have opted to obtain Ag_3PO_4 powders by reacting $AgNO_3$ with phosphate salts in aqueous solution since the co-precipitation technique provides narrow size distribution, prevents phase segregation, and inhibits agglomeration. The properties of three samples characterized by a variety of techniques are summarized in table.

X-Ray diffraction. The X-ray diffraction profiles of the synthesized samples indicate the presence of a single crystalline phase (Fig. 1). The have fairly narrow peaks and are therefore well crystallized. The patterns are indexed on the basis of a cubic unit cell in agreement with the JCPDS card no. 06-0505 (symmetry group *P*43*n*, no. 218). Silver orthophosphate crystallizes in an unusual structure where each Ag^+ is octahedrally coordinated by four oxygen atoms at 0.234 nm and two at 0.288 nm. The lattice constants are given in table along with the main physical properties of the three samples. Silver has a relatively low affinity for oxygen but forms complexes with elements of Group IV of the Periodic Table with an appreciable covalent character. The length of the P=O bond (0.16 nm) is large, leading to ~0.2 π bond per 1.0 σ bond [15]. The crystallite size (*D*) was obtained from the broadening (β) of the most intense XRD peak using the Scherrer equation:

$$D = \frac{0.94\lambda}{\beta\cos\theta}, \quad (1)$$

where θ is the diffraction angle. As shown in Fig. 1, the (210) peak was used to estimate the crystallite size. The *D* values 77, 63, and 62 nm, were obtained for PA1, PA2, and PA3, respectively. The crystallinity of the samples indicates the possibility for achieving submicron particles via soft-chemistry approach. This may require further improvement of the current chemical technique.

Morphology. Growth of Ag_3PO_4 is achieved by nucleation followed by agglomeration [16]. The precursor concentration and the reaction temperature are two crucial factors governing the nucleation process. The SEM micrographs show grains with different sizes and shapes for PA1 (Fig. 2). Particles with flat facets are also observed, presumably ascribed to the short reaction time. Grains with slightly larger dimension (~1 μm) and more or less regular shapes are observed for PA2 (KH_2PO_4) powder. By contrast, PA3 consists of regular grains with an average size of ~10 μm. The EDS spectra (Fig. 3) revealed the presence of all elements present in the silver orthophosphate, and the resulting compositions were consistent with the chemical formula. The sample synthesized from Na_2HPO_4 (pK_a ~12.67) exhibits the narrowest size distribution. This is ascribed to the pH solution where the specie is released slowly and the reaction occurs at relatively lower rate. This could provide the possibility to stop the particle growth earlier and to have lower size distribution.

Thermal analysis. The thermograms shown in Fig. 4 indicate that the conversion of amorphous powder into crystalline Ag_3PO_4 in all samples starts at room temperature. For the sake of clarity, we report here only the data for PA1 since no significant differences

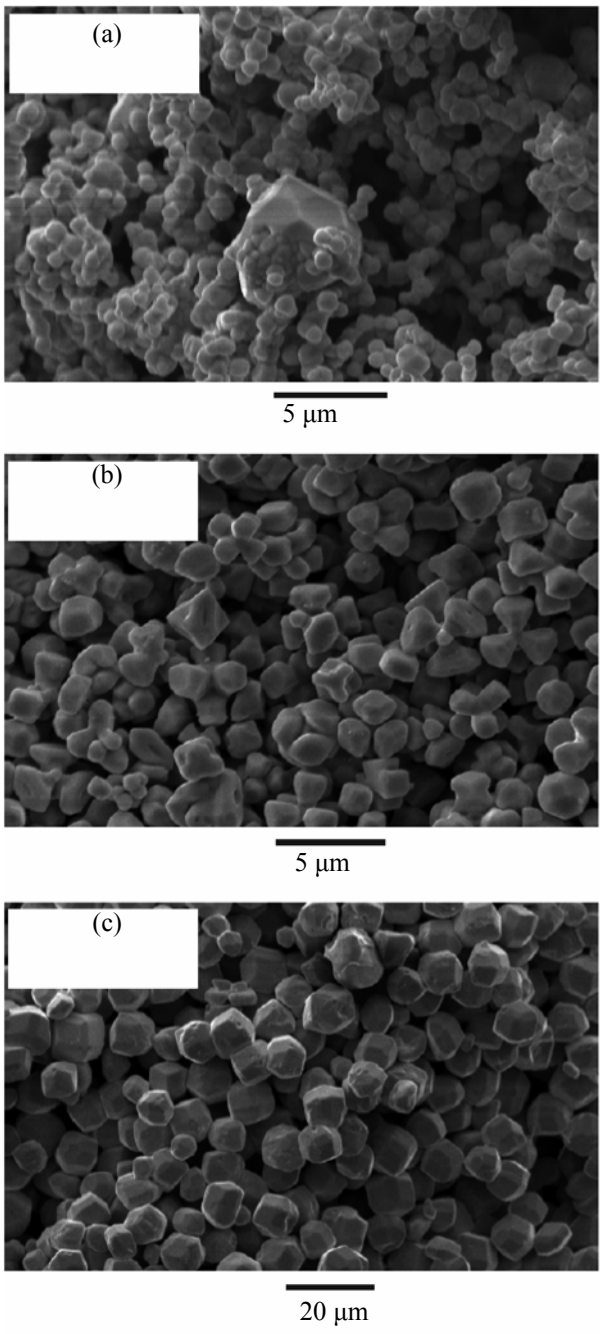

Fig. 2. SEM micrographs of (a) PA1, (b) PA2, and (c) PA3.

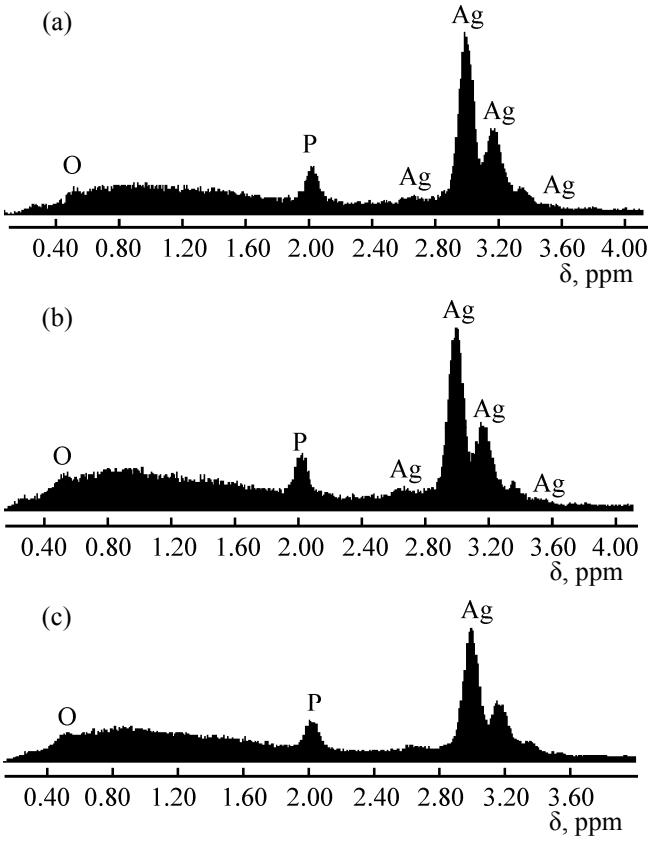

Fig. 3. EDS spectra of (a) PA1, (b) PA2, and (c) PA3.

were observed with PA2 and PA3. Small differences in the TGA plots may be attributed to water loss. The PA1 powder is thermally stable, and there is no sign of decomposition up to 750°C (Fig. 4a). The peak at 520°C in the DTA plot (Fig. 4b) corresponds to allotropic transition to a high- temperature phase crystallizing in the γ-Na_3PO_4 type (cubic symmetry) but not to melting of the powder as previously claimed by Thomas et al. [14]; Ag_3PO_4 melts at higher temperature (849°C) [17]. It is worthwhile to outline that the X-ray diffraction pattern of the high-temperature phase was obtained at 610°C (JCPDS no. 30-1137), i.e., above the transition temperature. To confirm the above stated, DSC measurement was undertaken (Fig. 5). In the heating plot, the endothermic effect at 520°C exactly equal to that obtained from DTA, is due to the crystallographic conversion. On the reverse scan, the exothermic peak shifts down to 475°C as a result of the reverse transition to the low-temperature phase.

FTIR analysis. The infrared spectra of Ag_3PO_4 samples (Fig. 6) are similar to those already reported in the literature [14]. The broad band at 1005 cm^{-1} is assigned to P–O stretching vibrations. The broad band between 2500 and 3700 cm^{-1} is attributed to various OH stretching vibration. This band broadened due to hydrogen bonding. The OH stretching vibration bands are likely to be related to P–OH groups, indicating the presence of by- products. Relatively weaker absorption bands are observed around 800 and 1650 cm^{-1} in the spectrum of PA3. These bands are attributed to

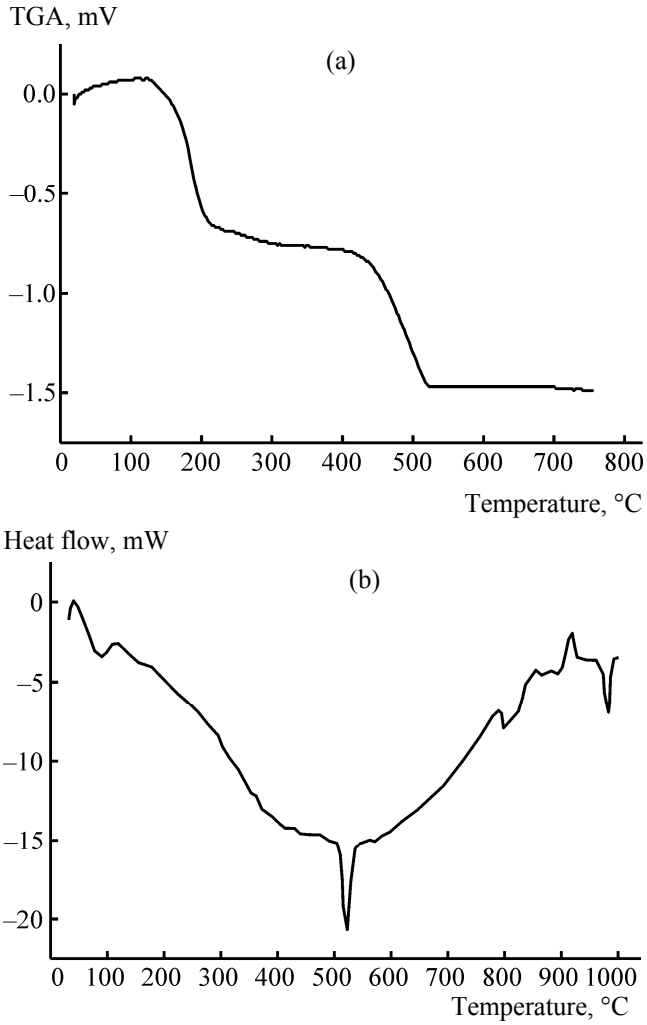

Fig. 4. (a) TGA and (b) DTA plots for silver orthophosphate powder (PA1).

vibrations of the PO_3 group. The peak centered at 1385 cm^{-1} in the spectra of PA1 and PA3 corresponds to vibration modes of some unreacted $AgNO_3$ [18]. A slight decrease of the vibration frequency ($\bar{\nu}$; see table) has also been reported elsewhere [19]. It is likely to result from displacement of Ag^+ toward oxygen ion in the distorted octahedral crystalline structure of Ag_3PO_4 powders, which shortens the Ag–O distance.

Optical properties. The optical gap (E_g) was determined from the diffuse reflectance spectra (Fig. 7) using the Munk-Kubelka function [20]:

$$F(R) = \frac{(1-R)^2}{2R} = \frac{k}{s}, \qquad (2)$$

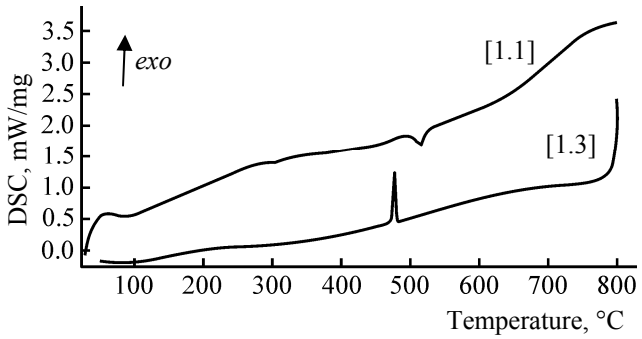

Fig. 5. DSC plot for Ag_3PO_4 powder obtained from Na_2HPO_4 (PA1).

where $R = I_{dif}/I_0$ is the diffuse reflectivity from an infinitely thick layer (about 2–3 mm), k is the absorptivity (cm^{-1}), and s is the scattering factor which is independent of the wavelength for particle sizes larger than the wavelength of the light; I_{dif} and I_o correspond to the diffuse and incident light intensities, respectively. The gap E_g is determined by extrapolating the linear portion of the $F(R)$ curve as a function of $(h\nu)^n$ to the $h\nu$ axis. The factor n corresponds to the transition type, $n = 2$ and 0.5 for direct and indirect transitions, respectively. In our case, the transition is directly allowed ($n = 2$). The gap E_g is found to vary from 2.30 eV for the powder with a size of less than 0.9 μm to 2.05 eV for a size of 1.5 μm (see table). However, we could not explain the eventual effect of the crystallite size on the optical properties. The optical emission of the quantized colloidal crystallites is blue shifted as the particle dimension increases. A similar trend has been observed for the FTIR peak positions. Such result indicates that PA3 (precursor H_3PO_4) with a lower gap absorbs more light over the visible region and can be attractive in photocatalysis.

Electrical conductivity. Silver orthophosphate powder integrated in solar cells must have a high conductivity (σ) to optimize electric charge collection. The conductivity measurement was performed using PA3. The conductivity is extrinsic in nature, and the charge carriers result from a slight deviation from the stoichiometry. The conductivity is thermally activated and follows an exponential law:

$$\sigma = \sigma_0 e^{-\frac{E_a}{RT}}. \qquad (3)$$

The capacitance measurement (figure not shown) indicated n-type behavior. The activation energy (E_a) calculated from the slope of the linear plot in Fig. 8 is found to be 0.2 eV, suggesting that the Fermi level

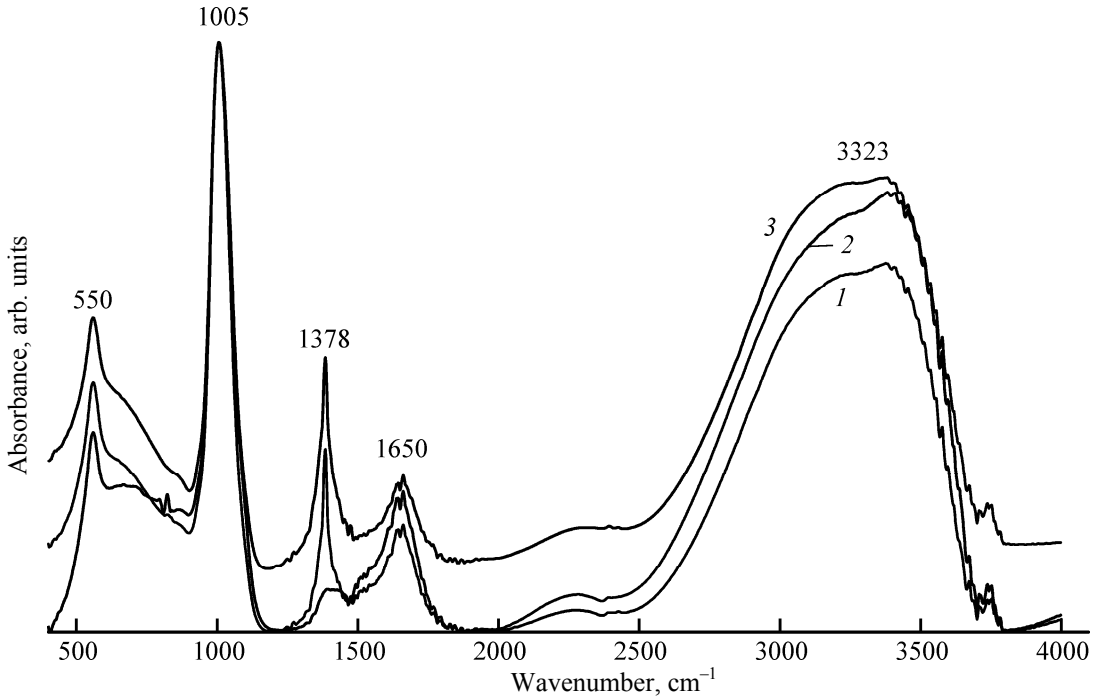

Fig. 6. FTIR spectra of (*1*) PA1, (*2*) PA2, and (*3*) PA3.

shifts toward the conduction band. Furthermore, we conclude that the conduction occurs via small polaron hopping. Therefore, variation of the conductivity is due primarily to the temperature dependence of the carrier density rather than to the mobility. The E_a value may explain the lower gap (2.05 eV) of PA3 due to higher impurity level. Work to evaluate the effect of the powder characteristics for the solar cells performance is underway and will be reported consecutively.

CONCLUSIONS

The aim of the present work was to elucidate how the phosphate precursor and its concentration affect the growth and physical properties of Ag_3PO_4 elaborated

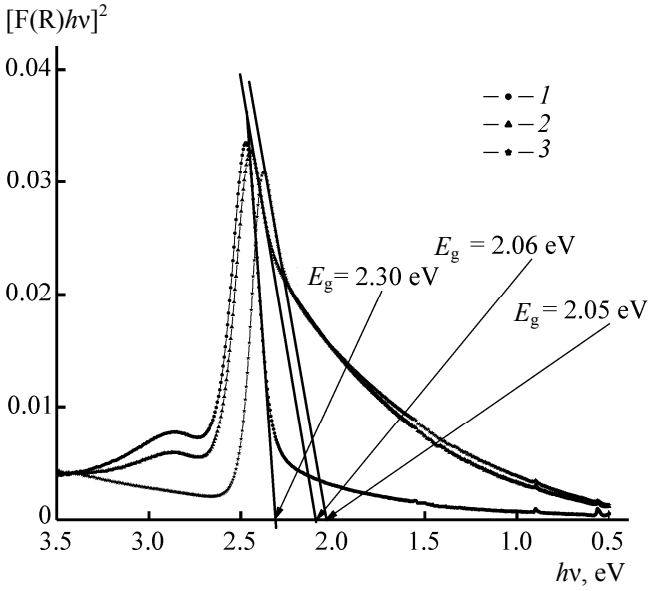

Fig. 7. Optical gaps of (*1*) PA1, (*2*) PA2, and (*3*) PA3.

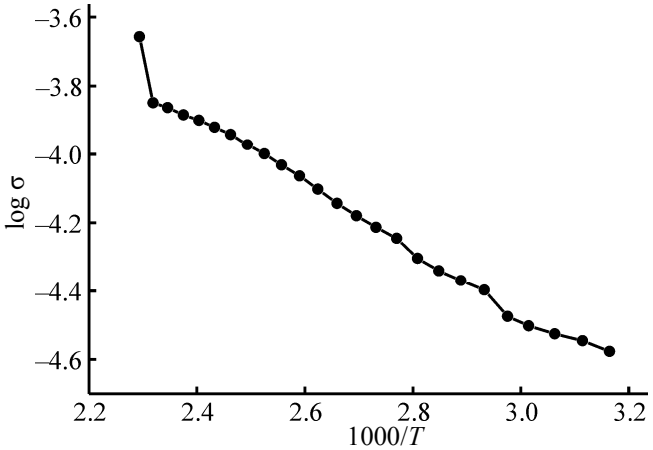

Fig. 8. Plot of electrical conductivity of Ag_3PO_4 powder (PA3) versus temperature.

by soft chemistry at ambient temperature. The powders have been characterized structurally and physically. The texture and morphology have been studied by X-ray diffraction and scanning electron microscopy, which showed that PA1 is well crystallized with smaller grains. The higher gap of the Ag_3PO_4 powder (PA1) obtained from Na_2HPO_4 as precursor is due to the lack of impurities. The soft chemistry synthesis described in this work will allow us to tune the solar cell properties as a function of the characteristics of silver orthophosphate powder.

ACKNOWLEDGMENTS

The authors thank A. Keffous, H. Menari, and S. Kermadi (Semiconductors Technology Research Centre for Energetics, CRTSE) for their support in the reflectance measurements, N. Souami (Algerian Nuclear Research Centre, CRNA) for his support in SEM/EDS analysis, and F. Bensebaa (National Research Council Canada, CNRC) for his help in editing the manuscript.

REFERENCES

1. Nijs, F., Poortmans, J., Sivoththaman, S., and Mertens, R.P., *IEEE Trans. Electron Devices*, 1999, vol. 46, p. 1948.
2. Schubert, G., Huster, F., and Fath, P., *PVSEC*, 2003, vol. 14, p. 441.
3. Rane, S.B, Khanna, P.K., Seth, T., Phatak, G.J., Amalnerkar, D.P., and Das, B.K., *Mater. Chem. Sci*., 2003; vol. 82, p. 237.
4. Rane, S.B., Seth, T., Phatak, G.J., Amalnerkar, D.P., and Das, B.K., *Mater. Lett*., 2003, vol. 57, p. 3096.
5. Wohlgemuth, J.H., Narayanan, S., and Brenneman, R.K., *Proc. 21st IEEE PVSC*, Kissimmee, 1990, p. 221.
6. Bruton, T., Mason, N., Roberts, S., Hartley, O.N., Gledhill, S., Fernandez, J., et al., *Proc. WCPEC-3*, Osaka, 2003, p. 899.
7. Ruby, D.S., Yang, P., Roy, M., and Narayanan, S., *Proc. 26th IEEE PVSC*, Anaheim, CA, 1997, p. 39.
8. Horzel, J., Szlufcik, J., Nijs, J., and Mertens, R., *Proc. 26th IEEE PVSC*, Anaheim, CA, 1997, p. 139.
9. Rohatgi, A., Hilali, M., Meier, D.L., Ebong, A., Honsberg, C., Carroll, A.F., et al., *Proc. 17th EU PVSEC*, Munich, 2001, p. 1307.
10. Porter, L.M., Teicher, A., and Meier, D.L., *Sol. Energy Mater. Sol. Cells*, 2002, vol. 73, p. 209.
11. Hilali, M., To, B., and Rohatgi, A., Abstracts of Papers, *14th Workshop on Crystalline Silicon Solar Cells and Modules*, Colorado, 2004, p. 109.
12. Bensebaa, F., *Nanoparticle Technologies: From Lab to Market*, Amsterdam: Academic, 2013, p. 429.
13. Yujie, D., Tong, D., Shiru, J., Long, J., and Fuping. L., *J. Membr. Sci*., 2006, vol. 281, p. 685.
14. Thomas, M., Ghosh, S.K., and George, K.C.., *Mater. Lett*., 2002, vol. 56, p. 386.
15. Wells, F., *Structural Inorganic Chemistry*, Oxford: Clarendon, 1975, 4th ed.
16. Khan, A., Qamar, M., and Muneer, M., *Chem. Phys. Lett*., 2012, vols. 519–520, p. 54.
17. Alekseev, V.N., *Kolichestvennyi analiz* (Quantitative Analysis), Moscow: Khimiya, 1972, 4th ed.
18. *Inorganic Library of FTIR Spectra*, Nicodom, 1998, vol. 3.
19. Alarifi, A., Deraz, N.M., and Shaban, S., *J. Alloys Compd*., 2009, vol. 486, p. 501.
20. Karvaly, B. and Hevesi, I., *Z. Naturforsch., Teil A*, 1971, vol. 26, p. 245.